Acoustic data from the spring 2011 bowhead whale census at Point Barrow, Alaska

C. W. CLARK[1], R. A. CHARIF[1], D. HAWTHORNE[1], A. RAHAMAN, G. H. GIVENS[2], J. C. GEORGE[3], AND C. A. MUIRHEAD[1]

[1]*Bioacoustics Research Program, Cornell Lab of Ornithology, Cornell University, Ithaca, NY 14850, U.S.A.*
[2]*Department of Statistics, 1877 Campus Delivery, Colorado State University, Fort Collins, CO 80523 U.S.A.*
[3]*North Slope Borough, Department of Wildlife Management, Barrow AK 99723, U.S.A.*

ABSTRACT

Arrays of bottom-mounted passive acoustic recorders were used to continuously record the sounds of bowhead whales migrating past Point Barrow, Alaska for a period of 105 days in April - July 2011, spanning the duration of the visual census. Recorders were deployed in a roughly linear array configuration near the edge of the shorefast ice bordering the open lead. The recorded acoustic data were analysed from 156 sample periods comprising a total of 331 hours coincident with the visual census. Bowhead sounds in the sample periods were found by manual inspection of multi-channel sound spectrograms of the array recordings. Source locations for bowhead sounds that were received on three or more sensors within the array were calculated using a robust localization algorithm. Very high levels of bowhead acoustic activity were observed in comparison to recording efforts undertaken during past censuses, including high rates of singing and call sequences. A total of 22,426 bowhead sounds yielded 15,647 reliable locations. Of these, 6,944 were within the rectangular aperture zone directly in front of the array and therefore used in the calculation of a new population estimate. The inclusion of these acoustic location data into the 2011 estimate of abundance is presented in SC/65a/BRG01.

INTRODUCTION

During the spring, bowhead whales, *Balaena mysticetus*, from the Bering-Chukchi-Beaufort (BCB) population migrate past Point Barrow, Alaska, USA, en route from wintering areas in the Bering Sea to summer feeding grounds in the Beaufort Sea.

Since 1984, the census of the BCB population during its spring migration past Point Barrow has included an acoustic monitoring component combined with a visual survey effort (Clark et al. 1986; Clark et al. 1996; George et al. 2004). In 2011, between 12 April and 7 June, the North Slope Borough's Department of Wildlife Management successfully completed a combined acoustic-visual census. The acoustic monitoring effort, conducted from mid-April through late July, used arrays of passive acoustic recording devices to continuously record underwater sounds. The objective of the acoustic study was to detect and locate vocalizing bowheads during a sub-sample of times in order to estimate the proportion of acoustically located whales that swam within 4 km of the perch from which the visual census was conducted.

This paper describes the methods used to collect and analyse the 2011 acoustic array census data, and provides a summary of bowhead acoustic activity and locations during selected sub-sample periods. The statistical analysis of the acoustic location data and the application of those data to an estimate of population abundance are presented by Givens et al. (2013, SC/65a/BRG01).

METHODS

Acoustic data collection

Recording arrays

Acoustic data were recorded using arrays of marine autonomous recording units (MARUs) developed by the Cornell Bioacoustics Research Program (Clark et al. 2010). A MARU consists of a digital audio recording system in a positively buoyant package that can be deployed on the bottom of the ocean for periods of many months. Once deployed, the recorder floats several meters above the sea floor, tethered to an anchor via an acoustically activated release device. A hydrophone mounted outside the sphere transduces sound pressure into an analog electrical signal, which is then filtered, digitized, and stored as a continuous series of time-stamped binary files on an internal hard disk. At the conclusion of a deployment, the recorder's acoustic release device is activated from a recovery vessel, causing the instrument to float to the surface for retrieval.

The MARUs used in this study were programmed to record continuously at a digital audio sampling rate of 2000 Hz. The effective acoustic bandwidth of the MARUs, accounting for effects of high-pass and low-pass filters, was 10 – 800 Hz.

A five-element array of MARUs was deployed late on 12 April 2011 in the nearshore lead system in the vicinity of the ice-based observation perch using a 6-m skiff with mixed success. The air temperature was -23° C making boat handling dangerous and dense ice prevented placing buoys more than ≈250 m north of the perch. An attempt was made to offset the recorders in a 'zigzag formation' along the lead edge. Two additional MARUs were deployed on 2 May 2011 by being dropped into the open lead from the nearshore ice edge. One of the five MARUs deployed initially was never retrieved. Because the audio data from differing number of MARUs were processed separately, we consider the four MARUs that were recovered from the set deployed on 12 April to comprise a four-channel array; these four plus the two that were deployed on 2 May comprise a six-channel array.

Relative positions and details of the individual MARU deployment sites are given in Figure 1 and Table 1. Depths at the deployment sites varied between 26 and 44 m.

Since the two MARUs deployed on 2 May were dropped directly from the ice edge, the line connecting their deployment sites was used to define the nominal ice edge for calculating offshore distances of whale locations; the actual ice edge was not perfectly linear. We define a rectangular zone directly in front of the array as the *aperture zone* (Figure 1). The aperture zone is the area within which the distribution of offshore distances of acoustic locations is used by Givens et al. (2013, SC/65a/BRG01). One end of the aperture zone is defined by the nominal ice edge. The sides of the aperture zone are perpendicular to the ice edge. The northern side of the aperture zone side intersects the ice edge at the northernmost MARU position; the southern side intersects the ice edge at a point midway between the two southernmost MARU positions. This midpoint is used, rather than the position of the southernmost MARU, because whale sounds with their first arrival on the southernmost MARU were excluded from the analysis, since the vast majority of these sounds are from distant whales approaching the array from the south. Their positions would be in the 30° "endfire" zone where locations tend to be highly unreliable. Since such locations are discarded later in the analysis process (see below), considerable time was saved in the initial data browsing by skipping such calls. However, if the aperture zone is defined as extending all the way to the southernmost MARU, the exclusion of calls with first arrivals on channel 1 would result in the omission of some locations between MARU 1 and 2. Using the midpoint between the two southernmost MARUs to define the edge of the aperture zone prevents this omission.

MARUs were retrieved on 27 and 29 July, after the sea ice had retreated from the deployment area. One of the seven units (site #5) deployed on 12 April failed to surface in response to the release command and was never recovered.

This is the first time that acoustic monitoring data have been collected beyond the end of the visual census period, which historically has been around 1 June, with end recording dates dictated by ice conditions and whale passage rates.

The four-element MARU array, which provided data for analysis from 0:00[1] on 13 April through 14:59 on 2 May had an array aperture of 4725 m, with distances between adjacent elements of 1638 to 1671 m. The six-element array, which recorded from 15:00 on 2 May through 12:00 h on 27 July, had an array aperture of 5065 m, with distances between adjacent elements of 755 to 1659 m. Given the rule of thumb that reliable acoustic locations can be calculated with a linear, sparse array out to ranges four times the array aperture (Carter 1993), these aperture values support our working assumption that acoustic locations calculated with these arrays are reliable out to approximately 20 km from the centre of the arrays.

Array synchronization

All of the MARUs were synchronized at the start and end of the deployment, and at repeated intervals during the recording period. Synchronization is required because the algorithm used for computing an acoustic location depends on precise and accurate measurements of the times at which the same sound was recorded by each MARU. Although the quartz-based oscillators that control the audio sampling rates in the MARUs operate at the same nominal frequency, small variations between individual oscillators lead to "clock drift" among MARUs in the array, which can substantially degrade the accuracy of the relative time-of-arrival measurements.

After recovery of the MARUs two methods were used to correct the digital audio files for the effects of MARU-specific clock drift. First, data from onboard temperature loggers were used to compensate for changes in clock frequency that occurred as a result of variations in temperature inside the MARU. Prior to deployment, the oscillator frequency of each MARU was characterized in the laboratory over a wide range of temperatures, yielding a MARU-specific curve of oscillator frequency as a function of temperature.

[1] All times are given in Alaska Daylight Time.

Table 1. Locations, depths, deployment and retrieval dates, for MARUs deployed near the visual observation perch in 2011. The MARU deployed at site 5 was not recovered. Approximate depths were obtained from Google Earth.

Site	Latitude (°)	Longitude (°)	Depth (m)	Deployment date	Recovery date
1	71.364067	-156.716650	37	12-Apr-11	27-Jul-11
2	71.355267	-156.763767	44	12-Apr-11	29-Jul-11
3	71.341383	-156.780300	40	12-Apr-11	29-Jul-11
4	71.332717	-156.818367	37	12-Apr-11	29-Jul-11
5	71.318367	-156.828800	26	12-Apr-11	(Not recovered)
6	71.330967	-156.795800	37	2-May-11	27-Jul-11
7	71.354533	-156.742783	31	1-May-11	27-Jul-11

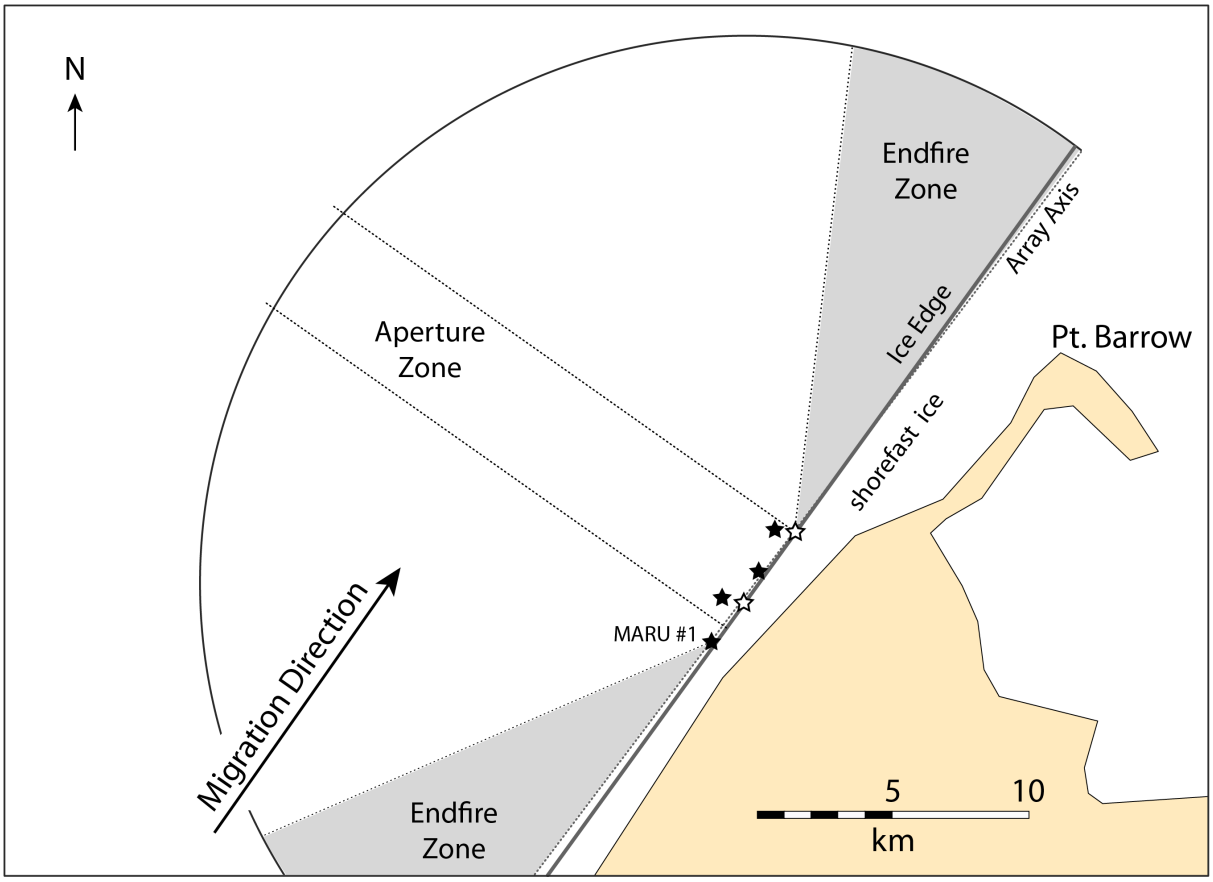

Figure 1**.** Passive acoustic arrays deployed near Pt. Barrow, Alaska. The filled black stars represent MARUs in the 4-channel array; open stars represent MARUs deployed on 2 May to make the 6-channel array. The large semicircle (radius = 20km) indicates the area within which acoustic locations were considered reliable. The nominal ice edge used for computing offshore distances is shown. The array axis and aperture zone (see text) are shown for the 6-channel array. For the 4-channel array, the array axis is tilted northward by 8°, and the aperture zone is slightly smaller than shown. The visual observation perch is located 190m from the northernmost MARU, too close to be shown separately at this map scale.

During the deployment period an onboard logger recorded the internal temperature at 15-minute intervals. After the MARUs were recovered, data from each unit's temperature log and its characteristic temperature-frequency curve were used to correct the stream of audio data so that the number of samples in each 15-minute temperature-logging interval matched the value predicted by the nominal sampling rate (Marchetto et al. 2012).

A second step in synchronizing recordings from MARUs relied on the use of synchronization sounds played into the water from known locations near the array at intervals of 1 to 8 days (mean = 5) during the deployment period. Because the times of the sync sound playbacks, the speed of sound, and the distances between the playback speaker and all of the MARUs are known, the expected arrival-times for the sync sound could be calculated for each MARU. After the MARUS were recovered and their data streams were temperature compensated, the observed arrival times of the sync sounds were compared to those expected. The number of audio samples between successive recorded sync sounds was adjusted by uniformly inserting or removing samples from the sound stream as necessary to bring the recorded sync sounds to the expected times.

Once all of the individual extracted audio data streams were time-compensated in these two ways, they were merged into synchronized, multi-channel audio files for subsequent analysis[2].

Analysis of acoustic data

Location analysis of the acoustic data was a four-stage process. First, experienced analysts inspected multichannel spectrograms for selected sample periods and logged bowhead whale sounds that were recorded on three or more MARUs for later location estimation. Sounds recorded on fewer than three MARUs cannot be located and were not logged. Second, an automated localization algorithm was run as a batch process on the logged whale sounds. Third, the acoustic locations (henceforth "locations") were screened by a combination of manual and automated processes to eliminate locations that were definitely or probably erroneous. Fourth, locations that were likely to be from the same whale were flagged by an automated algorithm in order to reduce bias from over-represented, acoustically active whales.

The selection of sample periods and the stages in the analysis process are explained in further detail below.

Selection of sample periods

Sample periods selected for location analysis were chosen with a two-step process. First, the season was divided into early (13-17 April), gap (18-21 April), core (21 April – 15 May), and late (16 May – 1 June) periods, based on major changes in visual sighting rates apparent in the visual field data. The gap period corresponds to about three days when no visual watch was possible due to storm conditions. A total of 230 hours of acoustic sample periods was selected, with 25, 15, 135 and 55 hours allocated to the early, gap, core and late periods. Aside from the gap period, all acoustic sampling periods were wholly contained within (potentially longer) periods with visual effort.

The second phase of sampling was designed after preliminary analysis of the visual and acoustic data from the first set of sample periods. In the analysis of Givens et al. (2013, SC/65a/BRG01), availability (the proportion of whales swimming within visual detection range) is estimated from the acoustic data as a smooth function of time. By looking at the preliminary estimated curve, it was possible to identify times when the standard error of the availability estimate was comparatively large. If, at this time, the estimated number of whales passing the perch was also high, then these two factors together could produce an undesirably large contribution of variance to the overall abundance estimate. To reduce this effect, an additional 98 acoustic sampling hours were selected in such periods, both within and outside intervals of visual effort. Finally two additional hours were sampled during visual watch on the first day (13 April) and one additional hour on the last day (1 June) of the analysed season. These enabled estimation of the availability curve over the entire season so that no extrapolation was needed. In sum, 331 hours of acoustic data were sampled. This means that acoustic location analysis was performed for about 28% of the total time acoustically monitored during the analysed visual census period as defined by Givens et al. (2013, SC/65a/BRG01). A complete list of sample periods is provided in Appendix 1.

Manual examination of data and annotation of bowhead sounds

Experienced acoustic analysts used XBAT, a customized, open-source MATLAB-base software system (http://www.birds.cornell.edu/brp/software), to examine multi-channel spectrograms of the recorded audio data from each sample period, typically viewing data in the 20 - 600 Hz frequency band, one minute at a time. MARU sites within each array are numbered from south to north. Thus, channel 1 in the multichannel

[2] The acoustic data from each MARU are stored in one channel in a multi-channel data file. The term *channel* is thus used in this paper to represent the acoustic data from one MARU. Individual channels are identified by a number (e.g., channel #3), indicating the site within the array where the corresponding MARU was deployed.

spectrograms always displays data from the southernmost MARU; the channel corresponding to the northernmost unit is channel 4 or 6 (depending on which array was active at a given time).

Sounds that were recorded by three or more MARUs were potentially locatable, and were annotated by using a cursor to draw a box around the sound in the one channel that recorded the clearest arrival of the call (i.e. the *reference channel*). Data on the time and frequency boundaries of marked calls were stored in XBAT log files for later processing by the locator algorithm. Calls that were received on fewer than three channels were not logged because they cannot be located.

Three categories of bowhead sounds were marked by analysts (Clark and Johnson 1984; Würsig and Clark 1993):

- **Individual calls** (Figure 2A)**:** Each individual bowhead call that was not part of a call sequence or song (see below) was logged.
- **Call sequences** (Figure 2B)**:** A call sequence is a sequence of calls, typically frequency-modulated and of similar shape, at regular intervals (typically 1.5 – 3 s) apparently from the same source. Call sequences typically last 20 – 30 s. When call sequences occurred, analysts logged one individual call from each sequence, rather than each individual sound, in order to reduce over-representation of an individual whale in the final data set.
- **Song (**Figure 3**):** When bowhead song (Würsig and Clark 1993; Stafford et al. 2008; Delarue et al. 2009, Tervo et al. 2009) was detected, a single song note was logged once per clock hour. Individual bowhead songs may contain many tens of individual notes within the span of one to two minutes, and individual whales may sing continuously for many tens of minutes or hours at a time. Logging every song note or even a single note from every song could thereby result in orders of magnitude more locations for singing whales than non-singing whales.

In all but the first few sample periods analysed, analysts excluded sounds where the first arrival was on channel 1 (corresponding to the southernmost MARU), because whales producing these sounds would have been to the south of the visual observation perch, and well outside of the rectangular aperture zone used for the abundance estimate (Givens et al. 2013, SC/65a/BRG01).

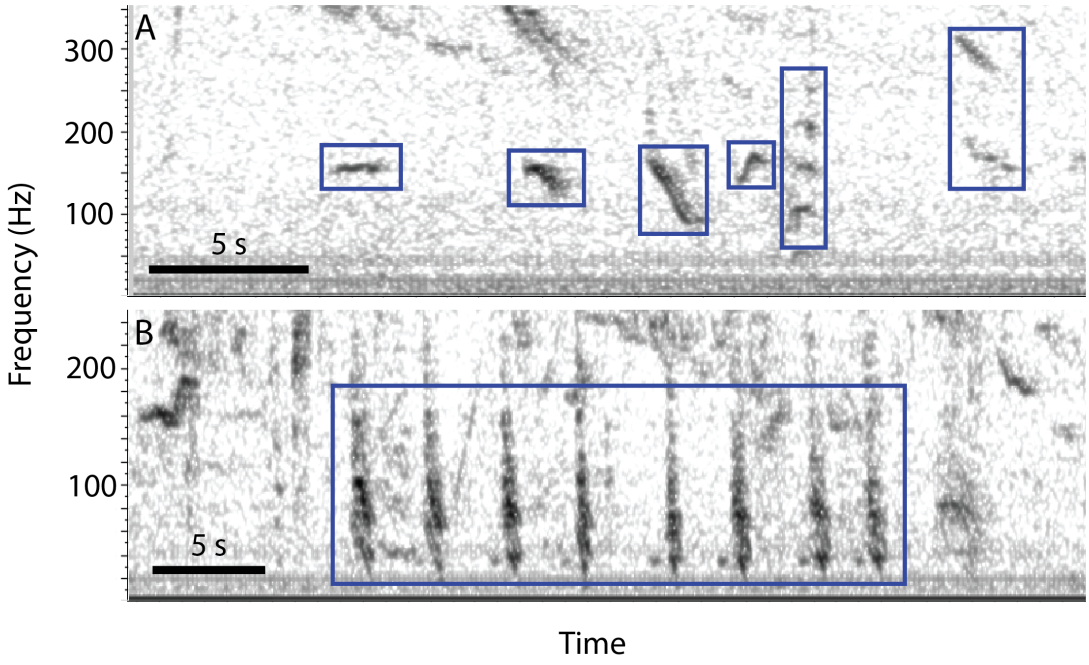

Figure 2. Examples of individual bowhead whale sounds. Only a single channel of audio recording is shown. (A) Individual calls recorded at 13:49 on 8 May. Note variability of call shapes. (B) A call sequence containing eight calls recorded from a bowhead whale at 23:10 on 29 April. Note the similar shape and regular time intervals of calls within the sequence.

Calculation of acoustic locations

When a sound is received on three or more sensors at known positions and in water of known sound velocity, the location of the sound source can be determined from the unique set of pairwise differences in sound's time of arrival at multiple sensors in an array (Clark et al. 1986; Clark et al. 1996; see Figure 4). In practice, sound source location accuracy and precision are compromised by several sources of uncertainty including sensor position, speed of sound, sound bandwidth and duration, and background noise (see Carter 1993).

The positions of vocalizing bowhead whales were calculated using a custom correlation sum estimation (CSE) algorithm (Cortopassi and Fristrup 2005), which determines the most likely set of pairwise time-of-arrival differences in order to determine the most likely source location. The CSE locator estimates the most likely set of time delays by finding the pairwise time lags which maximize the sum of filtered waveform cross-correlation values over all sensor pairs. This approach is equivalent to using near-field beamforming spatial energy maximization to estimate the location of an acoustic source (Appendix 2). The CSE locator software was configured to search for locations out to distances of 20 km from the centre of the array. Acoustic locations returned by the locator are expressed in Cartesian coordinates relative to the centroid of the sensor positions. The y axis of the coordinate system is oriented to geographic (true) North. The locator also returns heuristic estimates of the 95% confidence intervals for x and y coordinates (Appendix 3).

The location algorithms used in previous bowhead censuses determined pairwise arrival-time differences for the same sound recorded on different sensors by finding the maximum in the cross-correlations of, originally, the spectrogram images (Clark et al. 1986), and later, the filtered waveforms (Clark et al. 1996) of the recorded audio. In this approach, time delays are determined independently for each pair of hydrophones, based only on the peak value from the cross-correlation for the corresponding pair of audio channels. The pairwise arrival-time differences were then used as input to an algorithm that calculated the acoustic location (see Clark et al. 1996 for a more detailed description). In contrast, the CSE locator determines the most likely time delays by using all of the complete cross-correlation functions for all sensor pairs as an ensemble. This approach is more robust in the presence of noise than traditional peak-picking methods (Birchfield and Gillmor 2001, 2002).

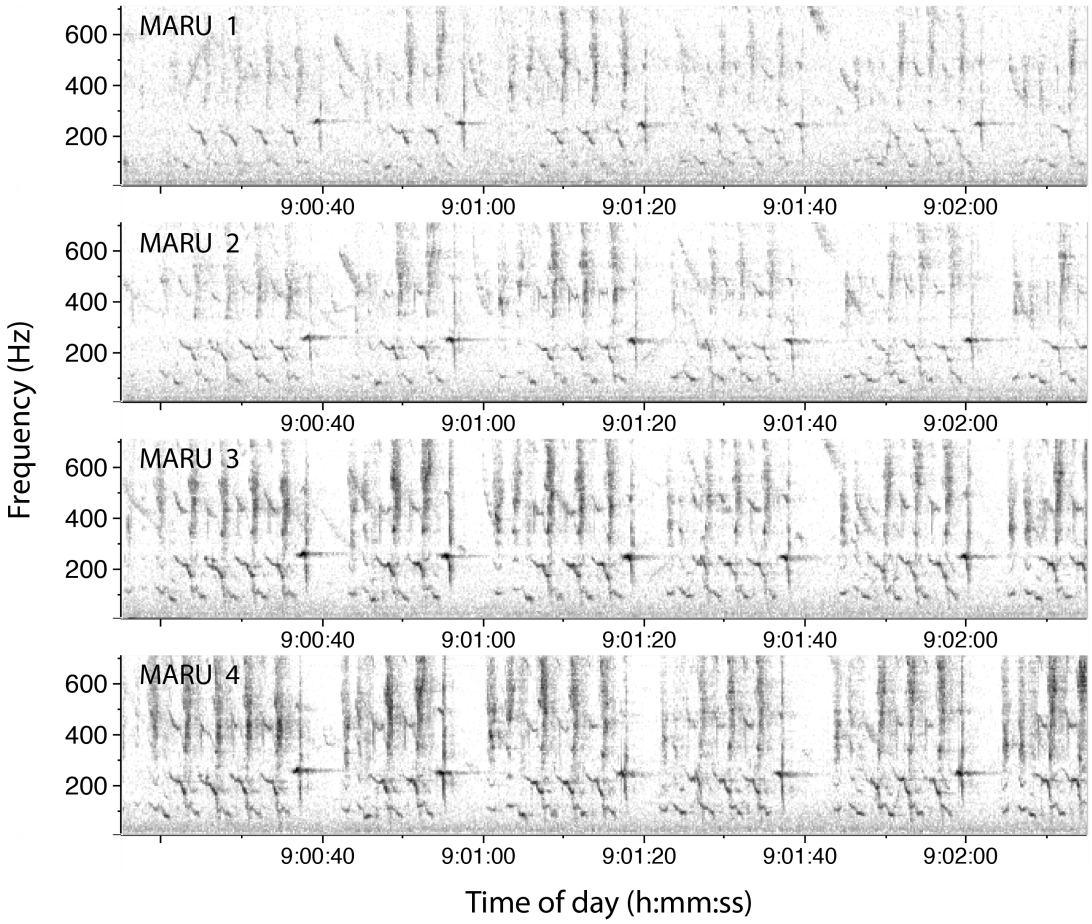

Figure 3. Example of bowhead whale song recorded at 9:00 on 13 April 2011. Two minutes of the recording are shown from all four MARUs in the recording array. MARU 1 is the southernmost reorder in the array (Figure 1). The highly repetitive structure typical of song is clearly visible.

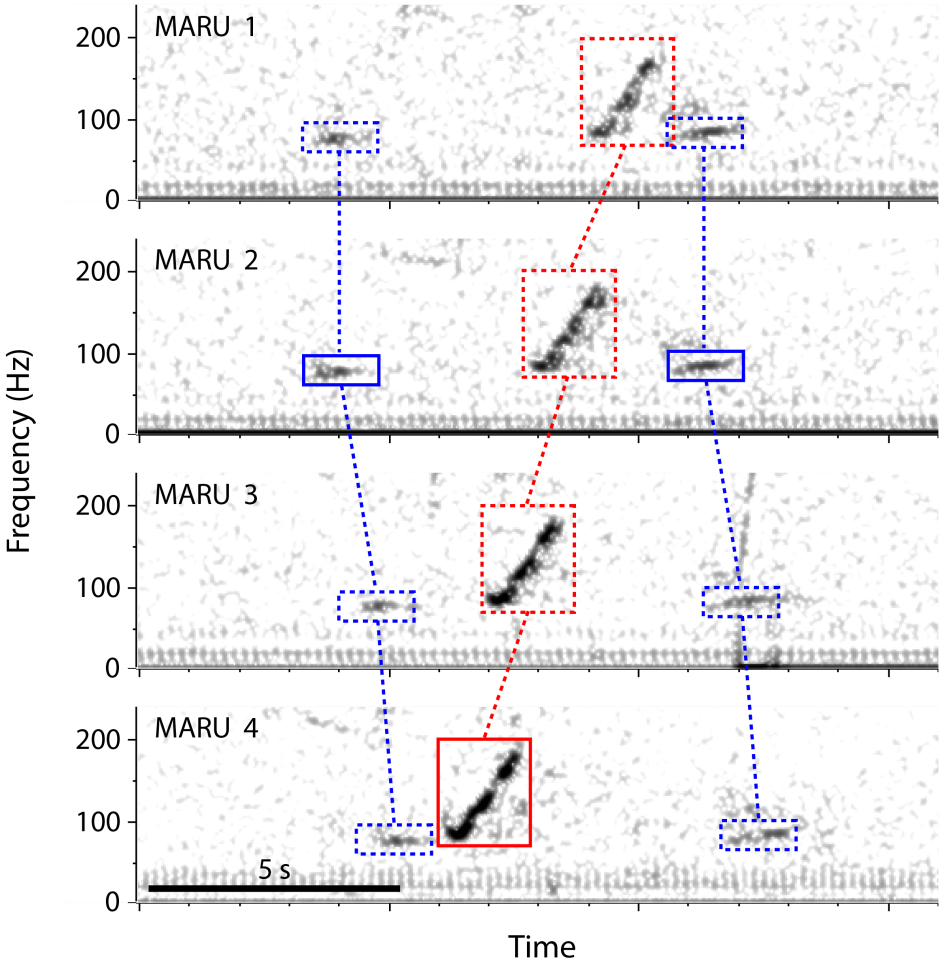

Figure 4. Time-of-arrival delays for three bowhead whale calls (boxes) received on the 4-channel recording array at 00:31 on 27 April. The four spectrograms represent synchronized audio streams from four MARUs, where MARU 1 is the southernmost recorder (see Figure 1). Solid outlines around calls were manually drawn in the "reference" channel for each call. Dashed outlines around calls in non-reference channels were drawn by the localization algorithm. Dashed lines link the same call as recorded on the four recorders. The order in which each call was recorded by the four MARUs is determined by the whale's distance from each recorder. The time delays of the first and third calls indicate that they came from approximately the same bearing, nearly equidistant between MARU 1 and 2. The time delays for the middle call indicate that it came from a different bearing, to the north of the array.

Review and filtering of automated locations

After all potentially locatable calls in a sample period were manually logged, locations were generated for the logged sounds. One of the outputs of the CSE locator is a prediction of the time at which the logged sound is expected to appear in all channels other than the reference channel, based on the estimated location. XBAT visualizes these predicted times of occurrence of secondary arrivals by displaying a coloured rectangular box overlaid on the spectrogram image in each non-reference channel (Figure 4). Analysts reviewed each location for faulty time-delays by inspecting the alignment between the predicted time-delay boxes and the images of the whale sound in the non-reference channels. Locations for which the time-delay boxes were improperly aligned were marked in the logs as unreliable and were eliminated from the final data files in a later post-processing step.

After locations were manually screened for faulty arrival-times, the following additional automated processing was performed via an Excel spreadsheet:

- Locations that fell outside of the 120° sector centered on the line perpendicular to the array axis were excluded from the data set (Clark et al. 1996). In general, with a nearly linear array, location estimates within

30° of the array axis tend to be unreliable with respect to range, hence are excluded from further analysis. These 30° sectors are called the `endfire zones' (Figure 1).

- Range and bearing errors from the centroid of the hydrophone array were calculated for all locations based on the heuristic 95% CIs for *x* and *y*. The *x* and *y* CIs define a rectangular uncertainty area centered on the estimated location. For range error, we use the difference in range between the estimated location and the farthest corner of this rectangle. For bearing error, we use half the difference between the bearings to the second and third nearest corners of this rectangle (Figure 5). With a linear array, range error generally increases with increasing range; bearing error is largely unaffected by range.
- Locations with bearing errors > 22.5° were flagged as unreliable and excluded from further analysis.
- Offshore distances and minimum and maximum offshore distances were calculated for all locations. The offshore distance for a location is the perpendicular distance from the location to the nominal ice edge (Figure 1). The minimum and maximum offshore distances are the perpendicular distances from the array axis to the nearest and farthest corners, respectively, of the location's uncertainty rectangle.
- Upon inspection of the complete set of located calls, it became apparent that many individual sounds had been logged for the same song and same call sequences, contrary to the planned protocol. As a result, a few sample periods contained inflated numbers of locations that were probably produced by the same individual whale in a small spatial area and a short period of time. In order to identify these extraneous acoustic events in the data set without a prohibitively time-consuming manual review of all events, we developed and applied a simple algorithm that identified sequences of events that occurred within 10 s of each other and that had overlapping range and bearing errors. Extensive spot-checking of the data marked by this algorithm indicated that most of the extraneous events were found by this process, with few cases of events being identified erroneously.

RESULTS

A total of 484 hours of audio data were recorded with the 4-channel array, from 11:00 on 12 April through 15:00 on 2 May. A total of 2067 hours of audio data were recorded with the 6-channel array from 15:00 on 2 May through 18:00 on 27 July.

A total of 331 hours of data were analysed, in 156 sample periods. In total, analysts marked 22,426 sounds that yielded locations in the 120° sector in front of the array. Of these, 3,195 were considered unreliable because their bearing errors were > 22.5°, and 4,393 were identified as likely 10-second duplicates. After removal of the latter two categories of events, a total of 15,647 locations remained. Of these, 6,944 were within the rectangular aperture zone directly in front of the array.

Figure 6 shows the temporal distribution of bowhead whale sounds. Across all 331 hours analysed, the mean rate of vocalizations was 51.2 sounds/h, including sounds for which locations were deemed unreliable because of excessive bearing error. The peak rate of vocal activity, 274 sounds/h, occurred between 8:00 and 10:00 on 2 May. The interquartile range in the cumulative distribution of locatable bowhead sounds was between 29 April and 9 May.

Recordings after 1 June have thus far not been systematically sampled to quantify bowhead acoustic activity. However, a few scattered bowhead calls have been observed in casual inspection of recordings during the period of 2 -10 June, indicating that some bowheads did pass through the census area after the conclusion of the visual census on 1 June.

Figure 7 shows the geographic distribution of the 15,647 bowhead sounds located in the 120° sector in front of the array, from the 331 hours of data analysed. Figure 8 shows the distribution of offshore distances of the 6,944 locations that were within the rectangular aperture zone.

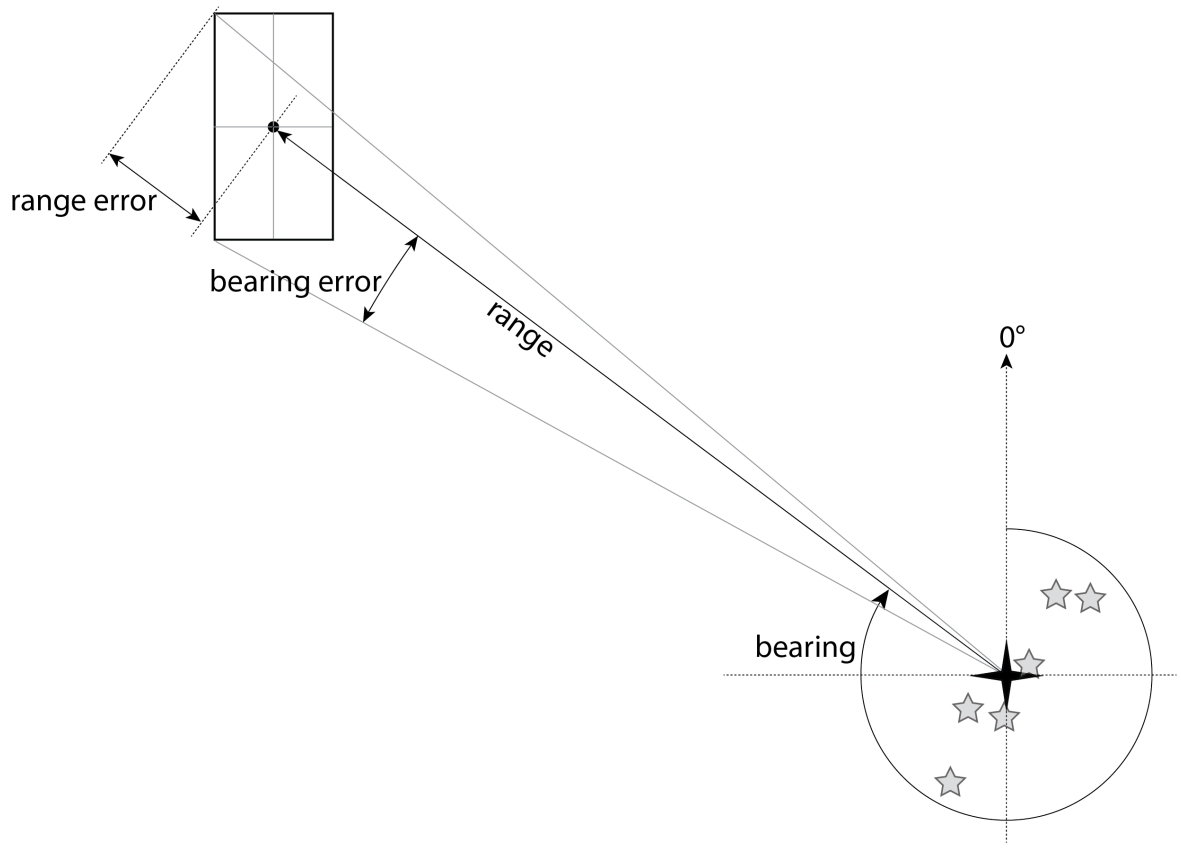

Figure 5. Schematic illustration of range and bearing to an acoustic location, and their respective errors. The gray stars represent the locations of the MARUs. The black cross represents the centroid of the recording array. The locator algorithm calculates the *x* and *y* coordinates of a vocalizing whale (black dot), and the heuristic 95% CIs for *x* and *y*, which define a rectangular uncertainty area. The range and bearing are calculated by converting the *x* and *y* to geographic polar coordinates. The range error is the difference between the range to the location and the farthest corner of the uncertainty rectangle. Bearing error is the difference between the bearing to the location and to either the second or third farthest corners of the uncertainty area.

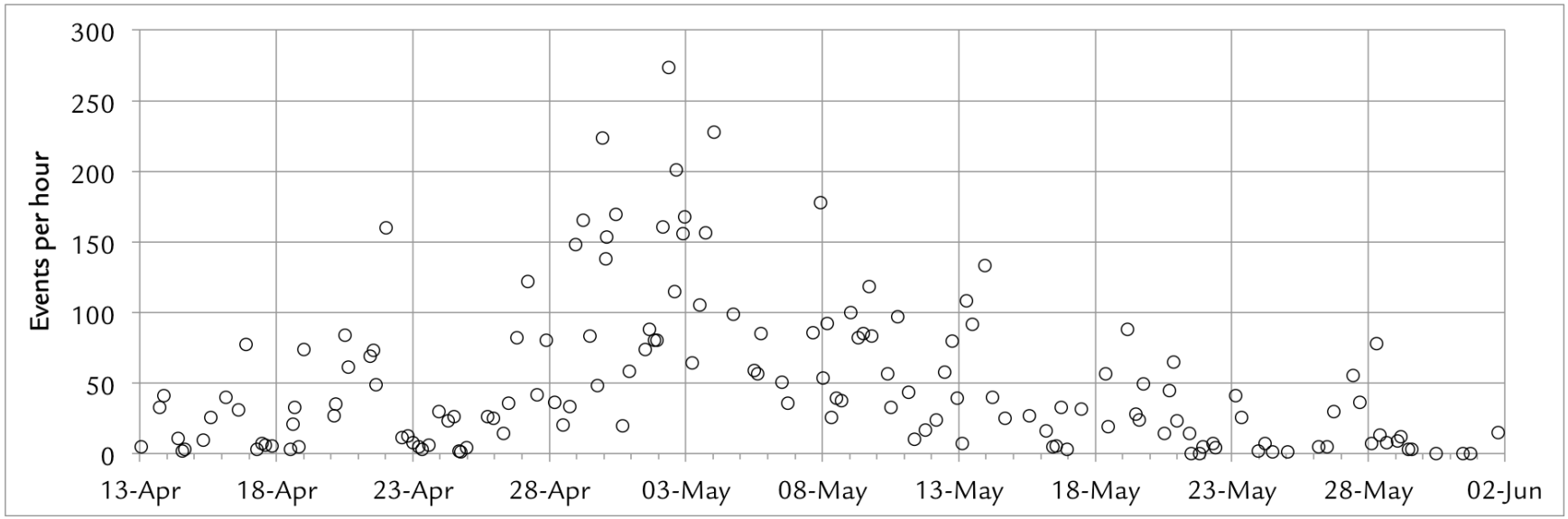

Figure 6. Mean rate of locatable bowhead whale vocalizations for 156 sample periods between 13 April and 1 June 2011. Each point represents one sample period. Mean length of sample period = 2.16 h. Vocalizations that were not locatable are not represented, but locatable sounds are included irrespective of estimated location error. "Duplicate" sounds that occurred within 10 s of another sound with overlapping range and bearing errors are omitted. Total number of sounds shown here = 18,033.

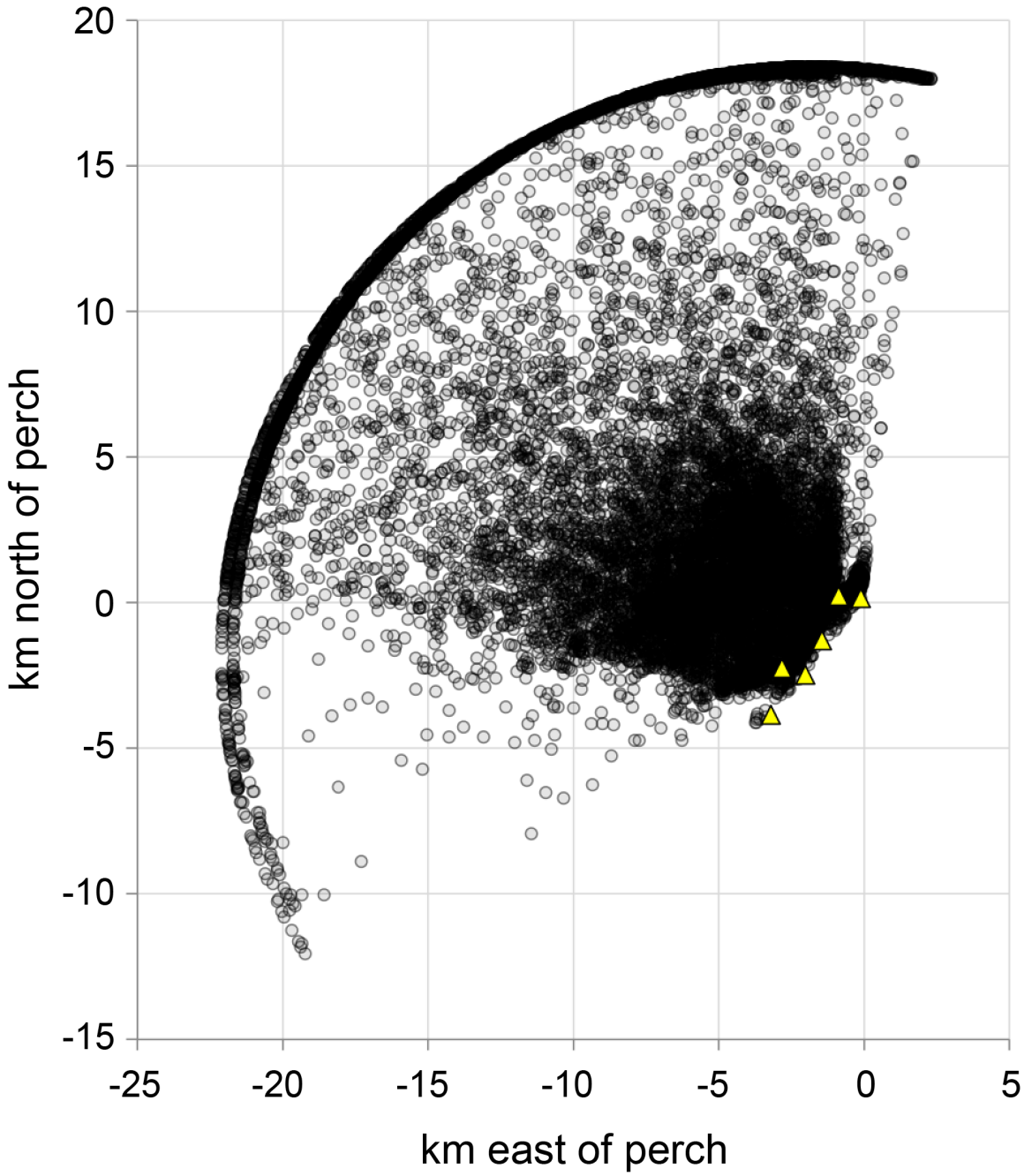

Figure 7. Acoustic locations of 15,647 bowhead sounds, from 156 sample periods totaling 331 hours of recording between 13 April and 1 June 2011. The origin of the coordinate system is the location of the primary visual perch. Triangles indicate locations of hydrophones in the 6-element recording array. As a whale's true location becomes farther away from the array, range errors inevitably increase. The locator software was configured to search for locations out to 20 km, which gives rise to the circular edge in the location distribution. Locations at or close to this 20 km represent whales that were probably beyond the 20-km search limit.

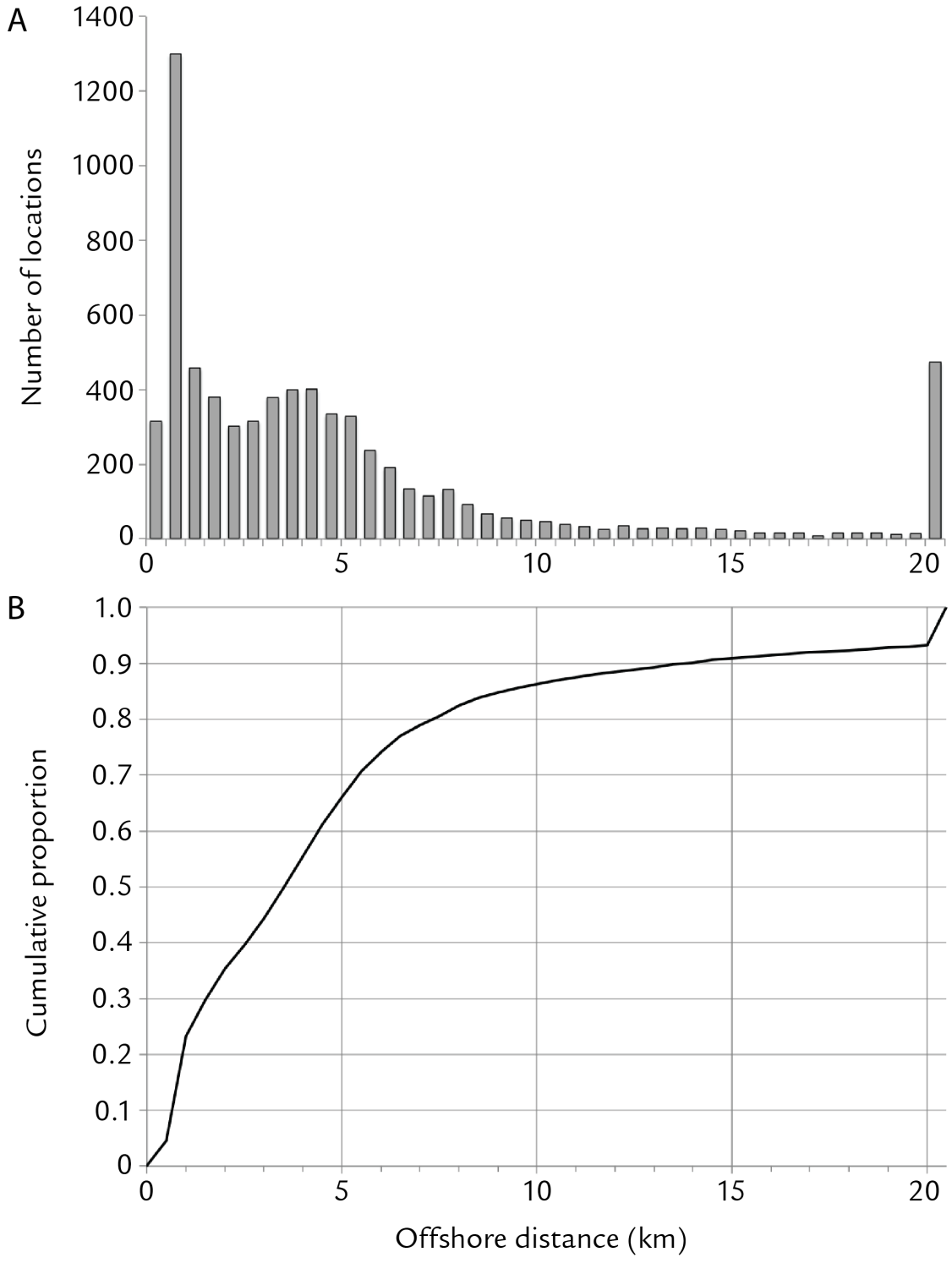

Figure 8. Offshore distance distribution for the 6,944 locations inside the rectangular aperture zone. (A) Number of locations in 0.5-km distance bins. (B) Cumulative proportion of locations ≤ a given distance. In both plots, the greatest value represents all locations at distance > 20 km.

DISCUSSION

Overall, in comparison to recordings from previous censuses, the array recordings made in 2011 had extremely high levels of bowhead whale acoustic activity. Table 2 compares mean rates of occurrence of locatable bowhead sounds in recordings analysed from the 2011 census to data from 1993 and 2001. Overall, between 1993 and 2011, the mean rate of acoustically located events increased by approximately 570%.

Table 2. Comparison of numbers of locatable bowhead whale sounds processed from censuses in 1993, 2001, and 2011.

	1993	2001	2011
Hours analyzed	732	757	331
Reliable locations	6,042	26,606	15,647
Locations / h	8.3	35.1	47.3

The 2011 recordings also appeared to have much higher occurrence rates of call sequences and songs compared to past censuses, although quantitative comparisons are not presently available.

There were some differences between the methods used in 2011 and in previous years, but we do not believe these difference account for the increase in acoustic activity or the number of reliable locations. These differences include the 2011 use of autonomous recorders suspended 2-3 m from the seafloor rather than cabled hydrophones deployed over the ice edge or through the ice as in all previous years. For the 2011 data the depths of hydrophones below the surface were 29-42 m, while in previous years hydrophone depths were typically 20-40 m. Recorder sensitivity in 2011 was less than that in previous years because MARUs were sampling at 2 kHz with a dynamic range of approximately 66 dB, while earlier systems were sampling at a minimum of 10 kHz with a dynamic range of 90 dB. If anything, we would then expect lower numbers of sound detections and fewer acoustic locations from the 2011 system compared to previous years. Array aperture differences were minimal between 2011 and previous years, where array aperture influences the range out to which locations are reliable. In 2011 array apertures were 4725 m (4-chann) and 5065 m (6-chann); in 1993 apertures of the 25 separate arrays used were typically around 4425 m. Thus, the 4- and 6-channel arrays used in 2011 were around 7% and 14% longer than those used in 1993.

We do not believe that any of these differences in field data collection and/or data processing methods can account for the almost 6-fold increase in rates of locatable sounds observed in 2011 in comparison to 1993.

ACKNOWLEDGEMENTS

We gratefully acknowledge the many researchers who worked on the ice-based visual and acoustic survey collecting the data required for the abundance estimate. In particular, we recognize Jason Michalec, Jason Herreman, Kate Stafford, and Billy Adams who helped deploy and retrieve the acoustic recorders under very dangerous conditions. We thank the Whaling Captains Association at Barrow and the Alaska Eskimo Whaling Commission for allowing us to conduct these studies near Barrow during the whaling season. We thank Kristin Hodge, Maureen Loman, Clara MacCarald, Elizabeth McDonald, and Kaitlin Palmer for painstaking analysis of the acoustic data. We thank Mike Pitzrick for software tools and consultation on post-processing of the location data. We also thank the North Slope Borough, NOAA, BOEM, and BP Exploration, Alaska, Inc. for funding by which to collect and analyse the acoustic data used for the abundance estimate.

LITERATURE CITED

Birchfield, S. T. and D. K. Gillmor. 2001. Acoustic source direction by hemisphere sampling. *IEEE International Conference on Acoustics, Speech, and Signal Processing (ICASSP)*. Salt Lake City, UT, USA, IEEE**:** 1-4.

Birchfield, S. T. and D. K. Gillmor. 2002. Fast Bayesian acoustic localization. *IEEE International Conference on Acoustics, Speech, and Signal Processing (ICASSP)*. Orlando, FL, USA, IEEE**:** 1-4.

Carter, G. C. 1993. *Coherence and Time Delay Estimation: An Applied Tutorial for Research, Development, Test, and Evaluation Engineers*, IEEE Press.

Clark, C. W., M. W. Brown and P. Corkeron. 2010. Visual and acoustic surveys for North Atlantic right whales, *Eubalaena glacialis*, in Cape Cod Bay, Massachusetts, 2001-2005: Management implications. *Marine Mammal Science* 26: 837-854.

Clark, C. W., R. A. Charif, S. Mitchell and J. Colby. 1996. Distribution and behavior of the bowhead whale, *Balaena mysticetus*, based on analysis of acoustic data collected during the 1993 spring migration off Point Barrow, Alaska. *Reports of the International Whaling Commission* 46: 541-552.

Clark, C. W., W. T. Ellison and K. Beeman. 1986. Acoustic tracking of migrating bowhead whales. *Oceans 86*, IEEE Oceanic Engineering Society**:** 341-346.

Clark, C. W. and J. H. Johnson. 1984. The sounds of the bowhead whale, *Balaena mysticetus*, during the spring migrations of 1979 and 1980. *Canadian Journal of Zoology* 62: 1436-1441.

Cortopassi, K. and K. Fristrup. 2005. A robust method for localization of animal sounds. *2nd International Workshop on Detection and Localization of Marine Mammals using Passive Acoustics*. Monaco.

Delarue, J., M. Laurinolli and B. Martin. 2009. Bowhead whale (*Balaena mysticetus*) songs in the Chukchi Sea between October 2007 and May 2008. *Journal of the Acoustical Society of America* 126: 3319-3328.

George, J. C., J. Zeh, R. S. Suydam and C. W. Clark. 2004. Abundance and population trend (1978-2001) of western Arctic bowhead whales surveyed near Barrow, Alaska. *Marine Mammal Science* 20: 755-773.

Givens, G. H., S. L. Edmondson, J. C. George, R. Suydam, B. Tudor and R. A. DeLong. 2013. Estimate of 2011 abundance of the Bering-Chukchi-Beaufort Seas bowhead whale population. Paper SC/65a/BRG01. *Scientific Committee of the International Whaling Commission*. Jeju Island, Korea.

Marchetto, P., A. Strickhart, R. Mack and H. Cheyne. 2012. Temperature compensation of a quartz tuning-fork clock crystal via post-processing. *Frequency Control Symposium (FCS), 2012 IEEE International*. Baltimore, MD, USA, IEEE**:** 1-4.

Stafford, K. M., S. E. Moore, K. L. Laidre and M. P. Heide-Jorgensen. 2008. Bowhead whale springtime song off West Greenland. *Journal of the Acoustical Society of America* 124: 3315-3323.

Tervo, O. M., S. E. Parks and L. A. Miller. 2009. Seasonal changes in the vocal behavior of bowhead whales (*Balaena mysticetus*) in Disko Bay, Western-Greenland. *Journal of the Acoustical Society of America* 126: 1570-1580.

Würsig, B. and C. W. Clark. 1993. Behavior (Chapter 5). In: J. J. Burns, J. J. Montague and C. J. Cowles (ed.), *The Bowhead Whale*, Special Publication Number 2, The Society for Marine Mammalogy**:** p. 157-199.

Appendix 1: Sample periods for acoustic analysis

Date	Start Time	End Time	Duration (h)	Date	Start Time	End Time	Duration (h)
13-Apr	0:00	2:00	2.0	27-Apr	4:00	7:00	3.0
13-Apr	15:44	18:30	2.8	27-Apr	10:18	16:18	6.0
13-Apr	20:00	22:00	2.0	27-Apr	20:00	22:00	2.0
14-Apr	8:32	10:32	2.0	28-Apr	4:00	6:00	2.0
14-Apr	12:38	13:38	1.0	28-Apr	10:00	14:00	4.0
14-Apr	14:34	16:34	2.0	28-Apr	16:00	20:00	4.0
15-Apr	6:38	8:38	2.0	28-Apr	22:00	23:59	2.0
15-Apr	13:12	15:12	2.0	29-Apr	4:00	7:00	3.0
16-Apr	3:00	4:00	1.0	29-Apr	10:00	14:00	4.0
16-Apr	13:30	15:30	2.0	29-Apr	16:00	20:00	4.0
16-Apr	20:30	22:30	2.0	29-Apr	22:00	23:59	2.0
17-Apr	6:15	8:15	2.0	30-Apr	1:00	2:00	1.0
17-Apr	11:00	12:00	1.0	30-Apr	2:00	3:30	1.5
17-Apr	13:00	16:17	3.3	30-Apr	8:30	12:30	4.0
17-Apr	20:03	21:00	0.9	30-Apr	14:30	18:30	4.0
18-Apr	12:00	13:00	1.0	30-Apr	21:00	23:00	2.0
18-Apr	14:00	15:00	1.0	1-May	12:00	13:00	1.0
18-Apr	16:00	17:00	1.0	1-May	14:08	18:12	4.1
18-Apr	18:00	21:00	3.0	1-May	20:00	21:00	1.0
19-Apr	0:00	1:00	1.0	1-May	22:00	23:59	2.0
20-Apr	2:00	3:00	1.0	2-May	2:00	5:00	3.0
20-Apr	4:00	5:00	1.0	2-May	8:00	10:00	2.0
20-Apr	12:00	13:00	1.0	2-May	13:00	14:59	2.0
20-Apr	14:00	17:00	3.0	2-May	15:00	16:00	1.0
21-Apr	10:00	11:00	1.0	2-May	21:00	22:00	1.0
21-Apr	13:00	14:00	1.0	2-May	22:00	23:59	2.0
21-Apr	14:55	16:05	1.2	3-May	4:00	7:00	3.0
22-Apr	0:00	1:00	1.0	3-May	10:00	14:00	4.0
22-Apr	10:30	18:00	7.5	3-May	15:00	19:50	4.8
22-Apr	19:00	21:00	2.0	4-May	0:00	1:00	1.0
23-Apr	0:00	0:15	0.3	4-May	17:00	18:00	1.0
23-Apr	5:00	6:00	1.0	5-May	10:10	14:00	3.8
23-Apr	8:00	9:00	1.0	5-May	14:40	15:15	0.6
23-Apr	10:10	18:00	7.8	5-May	16:17	20:00	3.7
23-Apr	22:00	23:59	2.0	6-May	10:10	14:11	4.0
24-Apr	6:00	8:00	2.0	6-May	16:01	20:00	4.0
24-Apr	10:00	14:00	4.0	7-May	14:00	17:00	3.0
24-Apr	15:00	18:00	3.0	7-May	21:00	23:59	3.0
24-Apr	18:00	19:00	1.0	8-May	0:00	2:00	2.0
24-Apr	22:00	23:59	2.0	8-May	3:00	5:00	2.0
25-Apr	16:00	19:00	3.0	8-May	7:00	9:00	2.0
25-Apr	22:00	23:59	2.0	8-May	10:49	14:03	3.2
26-Apr	7:00	9:00	2.0	8-May	16:00	18:17	2.3
26-Apr	10:17	14:00	3.7	9-May	0:00	2:00	2.0
26-Apr	18:00	21:00	3.0	9-May	7:00	9:00	2.0

Date	Start Time	End Time	Duration (h)	Date	Start Time	End Time	Duration (h)
9-May	10:03	14:00	4.0	20-May	16:00	18:00	2.0
9-May	15:57	17:51	1.9	20-May	20:00	22:00	2.0
9-May	18:30	21:00	2.5	20-May	23:00	23:59	1.0
10-May	9:00	10:20	1.3	21-May	10:00	11:00	1.0
10-May	10:20	14:00	3.7	21-May	12:00	13:00	1.0
10-May	16:00	20:00	4.0	21-May	19:00	21:00	2.0
11-May	3:00	5:00	2.0	21-May	21:30	23:30	2.0
11-May	8:30	10:00	1.5	22-May	7:00	8:00	1.0
11-May	16:00	21:00	5.0	22-May	9:00	10:00	1.0
12-May	3:00	5:00	2.0	23-May	3:00	4:00	1.0
12-May	9:00	14:00	5.0	23-May	8:00	8:59	1.0
12-May	16:00	20:00	4.0	23-May	23:00	23:59	1.0
12-May	22:00	23:59	2.0	24-May	5:00	6:00	1.0
13-May	2:00	4:00	2.0	24-May	10:00	14:00	4.0
13-May	6:00	8:00	2.0	25-May	0:00	2:00	2.0
13-May	10:02	14:00	4.0	26-May	4:00	5:00	1.0
13-May	22:00	23:59	2.0	26-May	11:00	12:00	1.0
14-May	5:00	6:00	1.0	26-May	17:00	18:00	1.0
14-May	16:00	18:00	2.0	27-May	10:00	12:00	2.0
15-May	14:00	14:40	0.7	27-May	16:00	17:00	1.0
16-May	4:00	5:00	1.0	28-May	2:00	3:00	1.0
16-May	10:02	10:50	0.8	28-May	7:00	8:00	1.0
16-May	12:45	14:00	1.3	28-May	10:00	11:00	1.0
16-May	16:00	20:00	4.0	28-May	15:00	17:00	2.0
16-May	23:00	23:59	1.0	29-May	1:00	2:00	1.0
17-May	10:02	14:00	4.0	29-May	4:00	5:00	1.0
18-May	8:00	10:00	2.0	29-May	11:00	12:00	1.0
18-May	11:00	12:00	1.0	29-May	14:00	15:00	1.0
19-May	4:00	5:00	1.0	30-May	11:00	12:00	1.0
19-May	10:00	13:00	3.0	31-May	10:00	12:00	2.0
19-May	14:00	15:00	1.0	31-May	17:00	18:00	1.0
19-May	17:00	19:00	2.0	1-Jun	17:00	18:00	1.0
20-May	12:00	13:00	1.0	1-Jun	18:00	19:00	1.0

Appendix 2: The Correlation Sum Estimation algorithm

The correlation sum estimation (CSE) locator employs near-field beamforming spatial energy maximization to estimate the location of an acoustic source. The formulation here is mathematically similar to that employed by Birchfield and Gillmore (2001, 2002) to study the localization of acoustic sources in a room, although here we compute bearing and range rather than azimuth and elevation as computed by those authors. Given N sensors, the average power output of an M sample record of a conventional delay and sum beamformer with a narrow band signal at frequency ω emitted from spatial location $\vec{x}$ is given by

$$P(\vec{x}) = \frac{1}{M}\sum_{k=1}^{M}\sum_{n=1}^{N}\sum_{m=1}^{N} y_n(k)y_m^*(k)e^{i\omega(\tau_n(\vec{x})-\tau_m(\vec{x}))}$$

where $\tau_n(\vec{x})$ is the propagation time from location $\vec{x}$ to sensor n, and $y_n(k)$ is the signal received at sensor n at discrete sample time k. Observing that in the phasor domain, the complex exponential represents a time shift operator, and exchanging the order of the summations, we may write

$$P(\vec{x}) = \frac{1}{M}\sum_{n=1}^{N}\sum_{m=1}^{N}\left[\sum_{k=1}^{M} y_n(k)y_m^*\left(k-\frac{\tau_n(\vec{x})-\tau_m(\vec{x})}{T}\right)\right].$$

We observe that the quantity in brackets is the M point cross correlation of $y_n(k)$ and $y_m(k)$ evaluated at discrete sample time $\frac{\tau_n(\vec{x})-\tau_m(\vec{x})}{T}$. That is,

$$P(\vec{x}) = \frac{1}{M}\sum_{n=1}^{N}\sum_{m=1}^{N} Corr(y_n, y_m)\Big|_{\frac{\tau_n(\vec{x})-\tau_m(\vec{x})}{T}}$$

where T is the temporal sample period. It is physically intuitive that the value of $\vec{x}$, which maximizes this sum, corresponds to the location of the source. One advantage to this technique is that the entire set of pair-wise cross correlation functions may be pre-computed in the frequency domain using the Fast Fourier Transform (FFT), which is much more computationally efficient than computation in the time domain. When searching space for the point of maximum power, we merely look up the correlation values in a series of tables, requiring no further correlation computation. If the maximum value of a pair-wise cross correlation function does not exceed a prescribed threshold value, then that pair is excluded from the sum. If the number of remaining channels does not exceed a prescribed number, then failure is indicated and the calculation is aborted.

The remainder of the algorithm consists of a stochastic search over space to find the point of maximum average power. Initially, 30,000 points are randomly chosen inside a circle of radius R centred at the origin. The average power is calculated at each point and the point $\hat{\vec{x}}$ of maximum power is located. The centroid of the set $\sum \vec{x_i}$ is also computed. The procedure is iterated with the circle centered at the point of maximum power observed over all previous iterations and a radius equal to the centroid magnitude of the previous iteration. The procedure continues until the magnitude of the centroid is less than a prescribed value.

Appendix 3
Error Estimation in the Correlation Sum Estimation (CSE) Locator v2.3

Estimation of standard errors and confidence intervals for the location estimates produced by the CSE locator is extremely complex. Below, we describe a heuristic approach. An advantage of this approach is that it allows us to incorporate more sources of uncertainty, including statistical `process errors' beyond standard sampling/estimation error. A disadvantage is that there is no assurance that the resulting confidence interval actually has 95% coverage. Due to this concern, we refer to the intervals as `heuristic 95% confidence intervals' to distinguish them from 95% confidence intervals derived directly from statistical theory.

Although the true coverage probability of these CIs may be only approximately correct, a relatively large degree of coverage rate error can be tolerated for the present purpose. Specifically, for the population abundance estimate of Givens et al. (2013, SC/65a/BRG01), the CIs produced here are used only to estimate weights for time-smoothing probabilities that offshore distances exceed 4 km. The estimated smooth is fairly insensitive to the choice of weights. Furthermore, in any time interval (say, 1 h), let us suppose that the CI coverage probabilities are relatively inaccurate but such inaccuracies are not correlated with offshore distance. Admittedly this may be a strong assumption, but to the extent that it is true, the errors in the weights employed at the local smooth fit for this time interval would tend to cancel each other out, thereby leaving the smooth fit relatively unbiased.

Now we discuss the components of uncertainty reflected in our heuristic estimates of standard errors and confidence intervals for locations.

1. Sources of location error
   The major sources of error in the CSE locator algorithm are:

   a. Statistical error
      The CSE locator operates by maximization of the sum of pair-wise correlations of the array's sensors. The acoustic data from each sensor include noise. The statistical error measures how much the noise affects the location estimate.
   b. Error due to sensor positional uncertainty
      The CSE locator algorithm assumes that the locations of the sensors are known exactly; in reality, this is never true.
   c. Error due to variation in the speed of sound
      Like the sensor positions, the CSE locator algorithm assumes that the speed of sound is known with great accuracy. In marine environments this could become a significant source of error.
   d. Error due to uncertainty in the sensors' clock rates
      Clock rate uncertainty can be mitigated to some degree by aligning the sensor recordings with respect to a bang or an FM sweep, and amortizing the error uniformly across the sensor recordings between the start and end markers. De-convolving the sensor unit's oscillator crystal temperature history can also mitigate temperature-induce clock rate drift.

2. Error estimation

   a. Statistical location error
      The question here is "Given the (noisy) sensor data, how accurately do we know the location of the energy maximum?" Accordingly, our goal is to compute the variance of the energy maximum location estimator $\hat{\hat{x}}$. While searching for an energy maximum, the CSE locator maintains a list of the top 1000 highest candidate energies and coordinates. We estimate the location estimator variance by computing the sample variance of this set.

$$\sigma_x^2 = \frac{1}{N-1}\sum(x_i - \bar{x})^2$$

      The same approach is used for σ_y^2 and (optionally) σ_z^2.

      Confidence intervals for x, y, and z are constructed independently using Gaussian assumptions. (The possible alternative approach based on a histogram of the 1000 candidates is a topic for future work.)

We have not yet implemented a non-independent approach based on a multivariate Gaussian approach for the three coordinates jointly.

b. Systematic location error due to sensor position uncertainties

Systematic error due to sensor position uncertainty is estimated using numerical sensitivities of the error maximum with respect to small changes in the sensor positions. To obtain the coordinate confidence limits, we employ a first order Taylor expansion of the energy as a function of location vector $\vec{x}$:

$$E = E(\vec{x}^{max}) + \delta\vec{x} \cdot \nabla_{\vec{x}'} E(\vec{x}')|_{\vec{x}'=\vec{x}^{max}} + \text{higher order terms}$$

Taking, for example, the x component, to first order we have

$$E = E(\vec{x}^{max}) + \delta x \frac{\partial}{\partial x'} E(\vec{x}')|_{\vec{x}'=\vec{x}^{max}}$$

Unfortunately, for a true maximum of the energy function, the derivative $\frac{\partial}{\partial x'} E(\vec{x}')|_{\vec{x}'=\vec{x}^{max}}$ is zero. However, the first order representation is linear in δx, approximating the energy surface as a cone with the constant slope along each coordinate axis. Therefore, if we choose a suitable point away from the energy maximum at the apex of the cone, we can numerically estimate the partial derivative $\frac{\partial}{\partial x} E(x)$. Conveniently, the CSE locator supplies us with an appropriate distance scale, the median centroid distance, d. We choose to compute the numerical derivative at distances $\Delta x = \Delta y = \Delta z = \frac{d}{2}$ from the energy maximum.

Numerical calculations of the derivatives can be very difficult to compute; the simple two point $\frac{\Delta y}{\Delta x}$ is frequently not accurate enough and it gives no bounds on the accuracy. Ridder's method was chosen to compute the derivatives and a bound on their errors. Conceptually, Ridder's method computes the ratio $\frac{\Delta y}{\Delta x}$ for a decreasing series of Δx and extrapolates to $\Delta x = 0$. If the error bound returned by Ridder's method is larger than 1% of the derivative estimate, the CSE locator displays a warning message but does not signal failure.

We seek to compute the sensitivity of the source location with respect to the change in sensor position location $\vec{s}_i$. Concentrating on the x component of the i[th] sensor position vector and invoking the chain rule for partial derivatives

$$\frac{\partial x}{\partial s_{i,x}} = \frac{\partial E}{\partial s_{i,x}} \frac{\partial x}{\partial E}$$

$$\frac{\partial x}{\partial s_{i,x}} = \frac{\frac{\partial E}{\partial s_{i,x}}}{\frac{\partial E}{\partial x}}$$

This is the sensitivity of location coordinate, x, with respect to the i[th] sensor position coordinate $s_{i,x}$. The partial derivatives appearing in the numerator and denominator are estimated using Ridder's method. For a finite uncertainty in the i[th] sensor position's x coordinate, $\Delta s_{i,x}$, we compute the change in x, Δx, to be

$$\Delta x = \frac{\frac{\partial E}{\partial s_{i,x}}}{\frac{\partial E}{\partial x}} \Delta s_{i,x} \quad ,$$

which is the error estimate we seek. Assuming we input the 95% confidence limit of $\Delta s_{i,x}$, we obtain the 95% confidence limit of Δx. The CSE locator repeats this calculation for the x, y and (optionally) z position components for each sensor used in the calculation of the energy (i.e. the correlation sum). A similar calculation is performed to obtain an estimate of the uncertainty in the location coordinates due

to uncertainty in the speed of sound. Finally, the errors are summed coherently by components to obtain an estimate of the upper bound of the uncertainty in the energy maximum location.

c. Systematic location error due to speed of sound uncertainty
The systematic error due to the uncertainty in the speed of sound is estimated using the same methodology used to estimate the systematic error due to uncertainties in the sensor locations.

d. Clock drift error
Due to temperature changes and aging of the crystal oscillators, MARU clocks may drift over time by rates of several seconds per day. MARU data extraction software mitigates the error in two ways: (1) oscillator temperatures are logged during the duration of the deployment and acoustic data are compensated for temperature drift using a function measured in the laboratory, and (2) any residual error is amortized over the interval between synchronization points. Amortization of a few seconds per day is actually a very small correction. For example, assume the clock drift was -3 sec/day. Since there are 86400 sec/day, we must insert one audio frame every $\frac{86400}{3} = 28800$ frames, a minor correction. By amortizing the error this way, we are never more than one sample period away from the correct absolute time. Therefore, we believe it is justified to ignore clock drift error.